

# THE FATIGUE GROWTH OF THREE-DIMENSIONAL FRETTING CRACKS

A. Cadario and B. Alfredsson

Department of Solid Mechanics, KTH (Royal Institute of Technology)

SE – 100 44 Stockholm, Sweden

alessandro@hallf.kth.se, alfred@hallf.kth.se

## Abstract

The fatigue growth of three-dimensional fretting cracks was investigated experimentally and numerically. Fretting experiments were performed with spherical contacts subjected to constant normal load, cyclic tangential load and constant or cyclic bulk stress. Crack detection methods based on strain gauges and acoustic emission measurements were adapted to the fretting experiment and allowed for estimation of the time for crack initiation and propagation. Fatigue crack growth was simulated numerically through a rapid few parameters crack growth description procedure. The crack path was separately predicted based on the direction of the largest principal value of the range stress tensor. The numerically computed fatigue lives and crack paths were compared to the experimental outcomes.

## Introduction

Fretting is a deteriorating process characterized by repeated small relative displacements (slip) in contacts that are loaded with cyclic tangential loads, see for example Hills and Nowell [1]. Slip develops within the contact and usually at the edge of it while stick conditions prevail in the remaining part of the contact. Fretting significantly accelerates the crack initiation process and the growth of short cracks. It must therefore be accounted for in the design process. Thus, effective engineering methods for fretting fatigue risk evaluations and accurate life predictions are needed. The analysis of fretting cracks is, however, a complex topic since the stick-slip contact conditions give rise to a non-proportional and multiaxial stress state. The three-dimensionality of the problem further complicates the growth analysis since, in principle, the crack growth should be followed locally along the crack front.

The present study investigates the growth of the three-dimensional fretting fatigue cracks that were observed in experiments with spherical contacts between titanium alloys.

## Experimental details

The fretting fatigue test sketched in Fig. 1 and presented in Alfredsson and Cadario [2] was utilized to reproduce fretting in controlled laboratory conditions. The contact took place between a spherical indenter and a plane specimen. The load system consisted of the normal contact force,  $P$ , the tangential force transmitted through the contact,  $Q$ , and the specimen bulk stress,  $\sigma_{\text{bulk}}$ . The experimental set-up allowed for separate control of the three loads. Two test types characterized by different loading conditions were studied. In the test type 1,  $P$  and  $\sigma_{\text{bulk}}$  were constant while  $Q$  was cyclic alternating with amplitude  $Q_a$ . A series of tests of type 1 were performed at different load levels. The flat specimen had a rectangular cross section of

$15 \times 7.5$  mm. The majority of the tests used an indenter of radius  $R = 400$  mm and a normal force  $P = 5.44$  kN. The cyclic tangential load amplitude varied between experiments from 1.415 to 3 kN and the bulk stress from 500 to 750 MPa. One test was also performed with  $R = 164$  mm,  $P = 0.9$  kN,  $\sigma_{\text{bulk}} = 750$  MPa and  $Q$  with amplitude 0.42 kN.

In the single reference test of type 2,  $P$  was constant while  $\sigma_{\text{bulk}}$  was cyclic, which in turn resulted in a cyclic in-phase  $Q$ . The specimen dimensions were in this case  $10 \times 5.5$  mm. The indenter radius was  $R = 190$  mm, the normal load was  $P = 1.2$  kN and the mean and amplitude values of the cyclic bulk stress were 273 and 78 MPa, respectively. The tangential force,  $Q$ , was measured during the experiments and ranged between  $-0.68$  kN and  $0.38$  kN with the negative peak at the time instant when  $\sigma_{\text{bulk}}$  reached its minimum during each cycle.

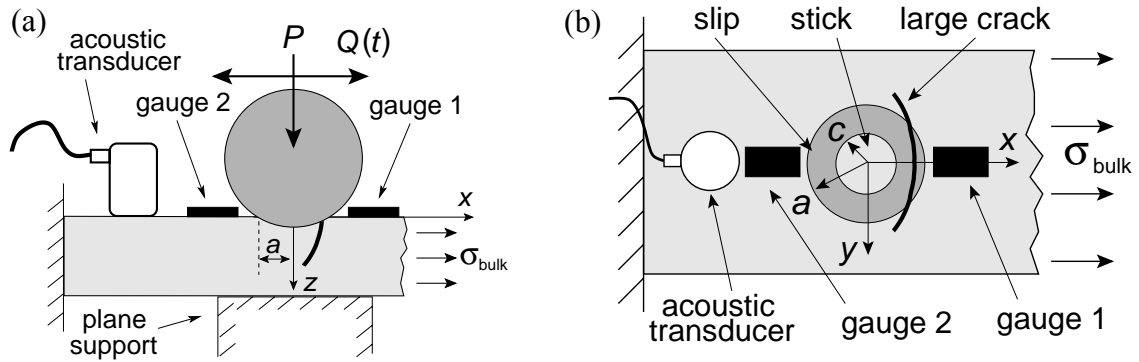


FIGURE 1. Schematics of the fretting experiment. (a) Lateral view. (b) Top view.

### Materials

Two  $\alpha+\beta$  titanium alloys were used in the experiments. The indenter was manufactured from Ti-6Al-4V and the specimen from Ti-17 which corresponds to a compressor blade-disc contact with Ti-17 as disc material. Alfredsson and Cadario [2] determine the static coefficient of friction in an unfretted dry contact and the steady state value in the slip zone to  $\mu_o = 0.45$  and  $\mu_n = 0.83$ , respectively. The fatigue growth data for Ti-17 were experimentally determined according to the standards ASTM E647 and to the constant  $K_{\text{Imax}}$  method, see Cadario and Alfredsson [3]. The growth data from the ASTM method appeared to be affected by crack closure at low load levels, while closure effects were absent in the data from the  $K_{\text{Imax}}$  method. The fatigue growth properties were described through exponential growth law

$$\frac{da}{dN} = C_9 \left( \frac{\Delta K_I}{\Delta K_{C9}} \right)^m, \quad (1)$$

where  $C_9 = 1$  nm and  $\Delta K_{C9}$  and  $m$  are material parameters.

### Crack detection

Cracks were detected during fretting tests by strain gauges and acoustic emission measurements. A strain gauge was positioned at either side of the contact along the  $x$ -axis, as is shown in Figs. 1. During the fretting tests, the gauges monitored any change in the strain field that could be related to the presence of a fretting crack.

Acoustic emissions measurements detected transient waves generated during crack propagation due to the rapid release of the elastic energy stored in the material at the crack tip. The waves propagated through the specimen and were detected by a piezoelectric transducer. An event was counted each time the signal from the transducer exceeded the threshold value. The event count was monitored during the experiments.

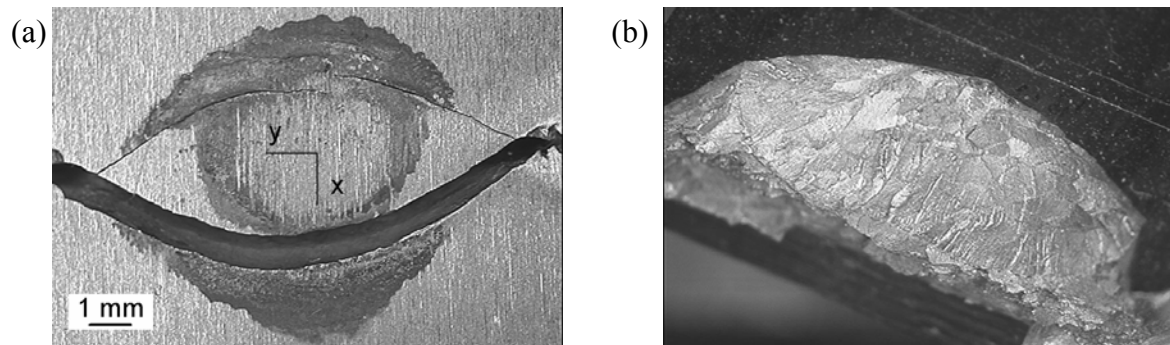


FIGURE 2. Type 1 crack after opening the specimen. (a) Top view. (b) Characteristic ellipsoidal crack shape.

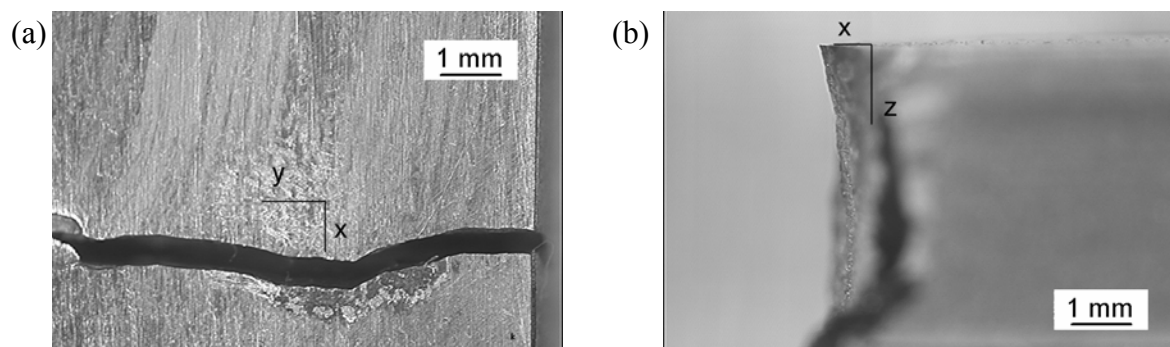


FIGURE 3. Type 2 crack after failure. (a) Top view. (b) Lateral view.

## Experimental results

A total of 28 tests of type 1 were performed. The experiments were halted at a predetermined number of load cycles. One or two symmetric large cracks were observed in almost all the fretting tests. The cracks were found at both positive and negative values of  $x$ . The tests resulted in 33 main fretting cracks of the type illustrated in Fig. 2a, where the top view of the contact region is displayed. In the figure, the annularly shaped fretting scar surrounds the central stick region with unaffected surface. After surface examination, the specimen was opened by an overload in order to study crack shape and initiation locations. The cracks always initiated within the slip zone. In most of the cases, the large fretting crack was in fact two cracks that had initiated at either side of the symmetry plane,  $y = 0$ , and then grown together. The fretting cracks then propagated towards the specimen edges and under the contact following a curved three-dimensional path. Fig. 2b displays a view of one large fretting crack. The cracks finally halted close to the plane  $x = 0$ . The geometry of the crack surface was determined through a series of Talysurf profiler measurements on the

experimental crack surface, see Fig 6a. By analysis of the reconstructed crack, it was found that the crack shape could be well approximated by a part of an ellipsoid.

In the single test of type 2, the specimen failed after approximately 300 kcycles. The crack initiated within the slip zone on the side closest to the bulk stress actuator and propagated towards the specimen edges and below the contact. Figs. 3a and 3b present top and lateral views of the fretting crack. In the top view, it is not possible to clearly identify stick and slip zones since it is believed that the contact slid during the test.

Fig. 4 presents crack detection results for both constant and cyclic bulk load. Fig. 4a shows an example of the minimum value of the cyclic radial strain measured by the two strain gauges during a type 1 test. Fig. 4b shows the accumulated number of events (total emission count) detected during the type 2 test.

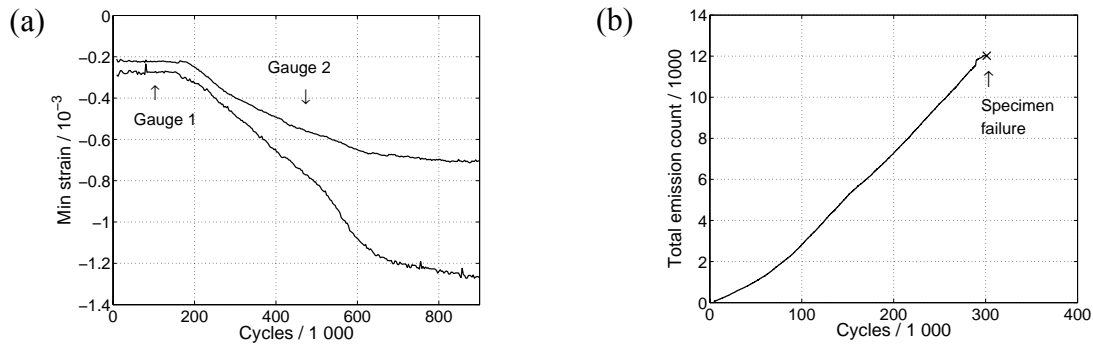


FIGURE 4. Crack detection measurements. (a) Minimum cyclic radial strains measured by two gauges in a type 1 test. (b) Total emission count in the type 2 test.

## Fatigue growth numerical procedure

By assuming that the crack propagated following the direction of pure mode I, the growth of the three-dimensional fretting crack was considered analogous to the growth of an equivalent plane edge crack loaded with the same mode I loading, see Cadario and Alfredsson [3]. The propagation of the fretting crack was simulated using an incremental procedure in which the crack growth rates were determined at each increment on the equivalent semi-elliptical plane crack. The ellipse semi-axes,  $s_1$  and  $s_2$  in Fig. 5a, represented the crack lengths in cross-sectional and top views, as are shown in Fig. 5b for a type 1 crack. During the incremental crack growth simulation, at the actual increment, the fatigue growth driving forces, *i.e.*  $\Delta K_I$ , were determined along the equivalent crack front using a  $K_I$ -database. Nilsson [4] compiles the  $K_I$ -database from a large number of FEM computations for plane elliptic edge cracks. To utilize the database, the stresses in the uncracked configuration at locations corresponding to the actual fretting crack were determined from an analytical elastic solution, see Cadario and Alfredsson [3]. Then, the stress component normal to the fretting crack surface was computed and transferred onto the equivalent plane edge crack. Finally, the  $K_I$  values were determined using the  $K_I$ -database. The crack growth rate at a point on the equivalent crack front was assumed to follow Eq. (1) in the direction normal to the crack front line. By least square approximation, see Nilsson [5], the equivalent growth rates were found in terms of  $s_1$  and  $s_2$ . The incremental crack growth,  $\Delta s_1$  and  $\Delta s_2$ , was then determined using a fixed time step and applied on the three-dimensional fretting crack, as shown in Fig 5b. The incremental growth direction was chosen so that the simulated crack front always lay on the experimental fretting crack surface. In a type 1 test, the fretting crack shape was approximated to a part of ellipsoid. In the type 2 test, the experimental crack had a limited curvature and its shape was

approximated to a plane elliptic surface crack. The incremental procedure was repeated until the simulated crack reached the same dimensions as the experimental one. The number of load cycles for crack propagation in a type 1 test with  $R = 400$  mm,  $P = 5.44$  kN,  $Q_a = 2.5$  kN and constant  $\sigma_{\text{bulk}} = 500$  MPa was numerically predicted to  $N = 180$  or  $N = 650$  keycycles with material data from constant  $K_{\text{Imax}}$  or ASTM tests, respectively. The number of load cycles for crack propagation in the type 2 test was numerically predicted to  $N = 75$  and  $N = 162$  keycycles with material data from the constant  $K_{\text{Imax}}$  and ASTM tests, respectively. Fig. 6 presents the crack shapes at the end of the simulations compared to the experimental cracks. Fig 7 displays the numerical crack growth rates expressed in terms of  $s_1$  and  $s_2$ .

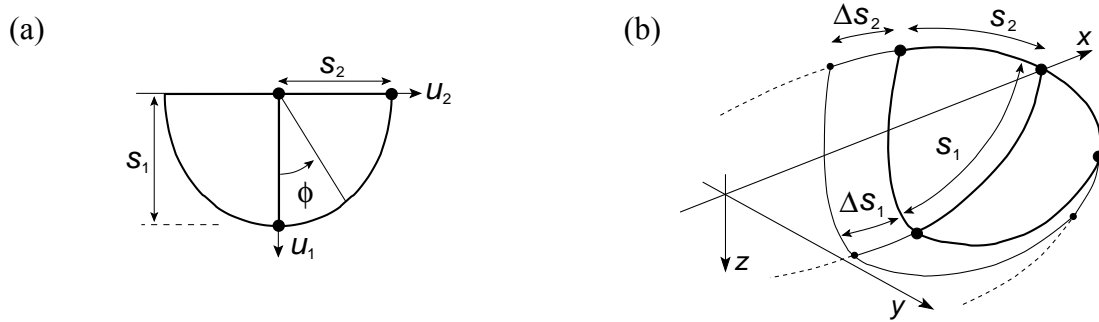


FIGURE 5. (a) Equivalent plane elliptic edge crack. (b) Ellipsoidal three-dimensional representation of the type 1 crack and incremental crack growth.

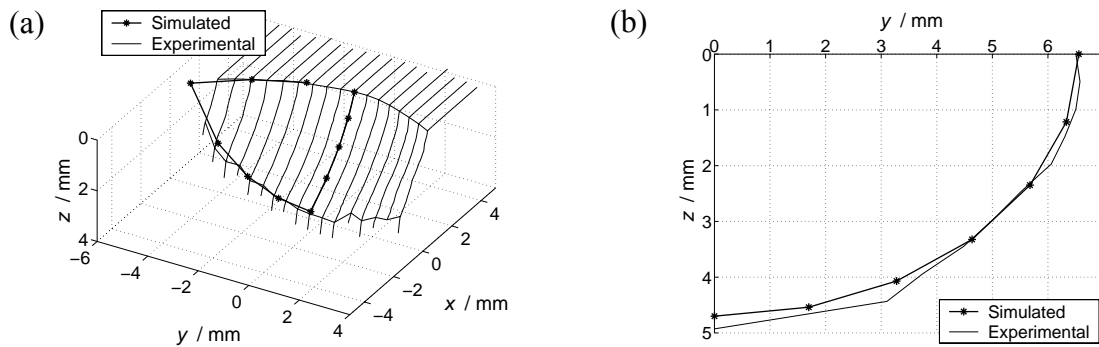


FIGURE 6. Comparison between simulated and experimental fretting cracks. (a) Type 1 crack from constant bulk test. (b) Type 2 crack from cyclic bulk test.

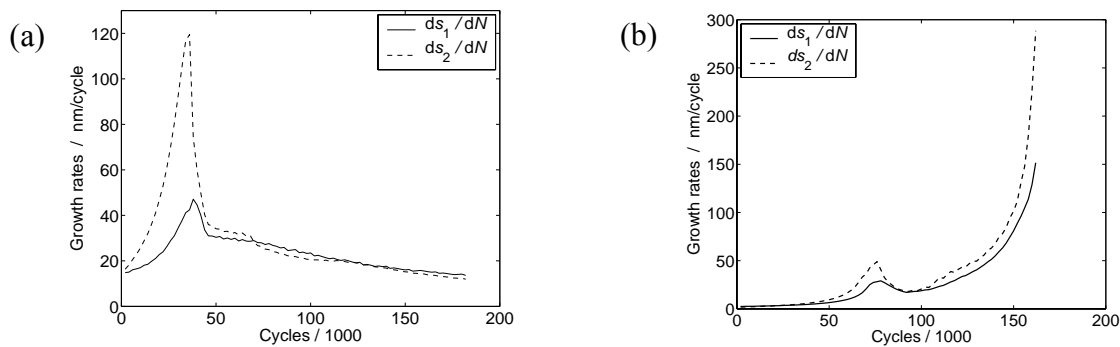


FIGURE 7. Growth rates estimations. (a) Constant bulk type 1 test. (b) Cyclic bulk type 2 test.

## Crack path estimation

The crack path estimation was carried out separately. It was assumed that the crack grew in the direction with the largest mode I stress intensity factor (SIF) range. The direction with the largest mode I SIF range was approximated with the direction perpendicular to the largest principal value of the stress range tensor  $\Delta\sigma_{ij}$ . The stress range tensor describes the cyclic variation of the stress components during the load cycle. The crack path was determined at the surface ( $z = 0$ ) and on the symmetry plane ( $y = 0$ ). The stress range tensor  $\Delta\sigma_{ij}$  was evaluated at the crack tip in the uncracked configuration. The direction of crack growth was then determined as the one orthogonal to the largest principal stress of  $\Delta\sigma_{ij}$ . The crack paths simulation was carried out incrementally starting at the location on the  $x$ -axis where the experimental crack met the contact surface. Fig. 8 compares the crack path estimations with the experimental cracks.

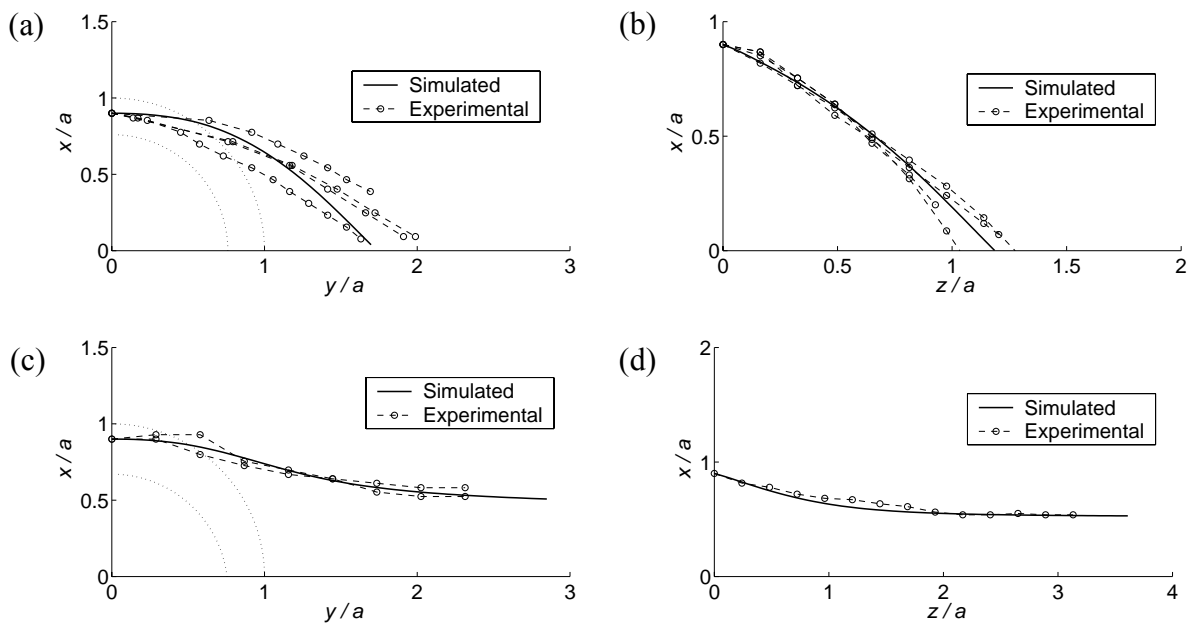


FIGURE 8. Comparison between simulated and experimental fretting crack paths. Type 1 test with  $Q_a = 2.5$  kN at (a)  $z = 0$  and (b)  $y = 0$ . Type 2 test at (c)  $z = 0$  and (d)  $y = 0$ .

## Discussion

The experimental results showed that a cyclic bulk stress is required for the fretting crack to continue growing to final failure. In fact, the fretting cracks produced with constant bulk stress always halted close to  $x = 0$ . The cyclic bulk stress, on the other hand, continued to drive the fretting crack also when the influence of the contact stresses diminished.

The strain gauges measurements during the type 1 tests showed that the surface strains decreased continuously during crack propagation, until they reached a steady state value when the crack halted, see the minimum radial strain in Fig. 4a. Crack detection by strain gauges furnished stable results in all the type 1 tests and it was always possible to detect the presence of a fretting crack. In the type 2 test, the strain gauge measurements did not provide clear results and no general trend could be coupled with a growing crack. A possible explanation is that the gauges were too far from the small contact region in combination with low load levels. In the acoustic emission measurements, if the background noise was constant

during a test, then crack growth was associated with an increase in the event count rate. Such an increase was clearly observed in the type 2 test, see Fig. 4b. In the type 1 tests, it was not always possible to relate the event count rate increase exclusively to crack growth. A probable reason for this is that the noise level was too high. Thus, the acoustic emission measurements could detect crack initiation and propagation but the results were not completely reliable.

Through strain gauges and acoustic emission, the experimental propagation lives could be estimated to be in the range from 170 to 500 kcycles in type 1 tests and to 225 kcycles in the type 2 test. The time for crack initiation was estimated to be in the range from 70 to 180 kcycles for both test types. This also indicated that the initiation process and the growth of short cracks were more influenced by the fretting loads than by the bulk stress.

In the fatigue growth simulations of type 1 tests, the cracks were always open during growth, *i.e.* the estimated  $K_{Imin}$  was positive along the crack front. Thus, the growth of fretting cracks occurred closure free and the material data obtained with constant  $K_{Imax}$  test were the most appropriate for the description of the growth rates. With material parameters from the constant  $K_{Imax}$  test, the numerical life estimate became 180 kcycles. Thus, a good numerical fatigue life prediction was obtained. The comparison of the simulated and the experimental crack shape in Fig 6a shows that the ellipsoidal crack form and the parameters  $s_1$  and  $s_2$  well described the fretting crack growth. The predicted crack growth rates, presented in Fig. 11a, show an initial accelerated crack growth, especially at the surface, which is driven by the high fretting loads. The growth rates reached a maximum value and then diminished as the crack front moved away from the contact region. Further growth then occurred at comparable rates at the surface and in cross section.

In the fatigue growth simulation of the type 2 test, crack closure was predicted when the crack was small through a negative value of  $K_{Imin}$ . As the crack grew longer,  $K_{Imin}$  became positive and the crack opened. If closure free material data were used, then a conservative numerical fatigue life was obtained. On the other hand, also the material data from the ASTM test gave a conservative fatigue life prediction,  $N = 162$  kcycles, as compared to the measured life,  $N = 225$  kcycles. A possible reason is that crack closure is underestimated in the numerical model. The good agreement between the simulated and the experimental crack shapes, presented in Fig. 6b, shows that the parameters  $s_1$  and  $s_2$  and the plane crack assumption well described the evolution of this fretting crack. The predicted growth rate in Fig. 7b had, also in this case, a peak when the crack was close to the contact region and then decreased as the crack front moved away from the contact. The growth rates increased again when the crack became larger.

The crack path predictions by the maximum hoop stress range on the planes  $z = 0$  and  $y = 0$  displayed in Figs. 8 show a good agreement with the experimental cracks. This further confirmed that the normal stresses were the main driving forces and that mode I dominated the growth of the long fretting crack. The larger discrepancies between estimated and experimental paths are observed close to the specimen edges for the type 1 test, see Figs. 8a and 8b. This was probably due to the half space assumption used for the finite specimen in the stress estimates. Any difference between estimated and experimental crack paths is much smaller in the type 2 test. In fact, at a certain distance from the contact, the crack growth was dominated by the cyclic bulk stress which was not influenced by edge effects since it acted in the specimen longitudinal direction.

## Conclusions

In the fretting experiments with constant bulk stress the fretting crack halted under the contact while it continued its growth to specimen failure in the cyclic bulk stress test. Thus, a cyclic bulk load is required for fretting fatigue crack growth to final component failure, given that the component dimensions are sufficiently large. The time to crack initiation and the fatigue propagation life could be experimentally estimated through strain gauges and acoustic emission measurements. The initiation period appeared to be similar for both the experiments types with constant and cyclic bulk stress. This implies that the contact loads, more than the bulk stress, influenced crack nucleation.

Crack path numerical simulations showed that the current fretting fatigue cracks followed the direction with the largest mode I load range for both cyclic and constant bulk load. The paths were well approximated by the direction perpendicular to the largest principal value of the stress range tensor  $\Delta\sigma_{ij}$  evaluated in the uncracked configuration. Utilizing mode I growth, the crack growth life of the fretting cracks was simulated with a few parameter crack growth procedure. The procedure rapidly produced estimates of the fatigue crack propagation lives of the three-dimensional cracks subjected to the complex fretting contact stress state.

## Acknowledgments

The work was funded by the Swedish Energy Authority and Volvo Aero. Dr. Thomas Hansson, Mr. Magnus Andersson, Tekn. Lic. Anders Skyttebol and Dr. Hans Jergeus are acknowledged for valuable discussions. The authors want to express their gratitude to Mr. Hans Öberg for the valuable help with the experiments. Bengt Möllerberg, Bertil Dolk and Johan Wikström manufactured the experimental rig and the specimens. Suggestions made by Prof. Fred Nilsson are much appreciated. The authors are also grateful to Dr. Stefan Björklund for the help with surface measurements.

## References

1. Hills, D.A., Nowell, D., *Mechanics of Fretting Fatigue*. Kluwer Academic Publishers, Dordrecht, 1994.
2. Alfredsson, B. and Cadario, A., To appear in: *Int J Fatigue*.
3. Cadario, A. and Alfredsson, B., Submitted to: *Engng. Fracture Mech.*
4. Nilsson, L., SAQ/FoU-Report 98/11. 1998.
5. Nilsson, F., *Int. J. Fracture*, vol. 54, 35-44, 1992.